

Document downloaded from:

<http://hdl.handle.net/10251/65016>

This paper must be cited as:

Impellizzeri, S.; Simoncelli, S.; Fasciani, C.; Marín García, ML.; Hallett-Tapley, GL.; Gregory K. Hodgson; Hodgson, GK.... (2015). Mechanistic insights into the Nb₂O₅ and niobium phosphate catalyzed in situ condensation of a fluorescent halochromic assembly. *Catalysis Science and Technology*. 5(1):169-175. doi:10.1039/C4CY00703D.



The final publication is available at

<http://dx.doi.org/10.1039/c4cy00703d>

Copyright Royal Society of Chemistry

Additional Information

Mechanistic insights into the Nb₂O₅ and niobium phosphate catalyzed in situ condensation of a fluorescent halochromic assembly

10 Stefania Impellizzeri,^a Sabrina Simoncelli^{a,b} Chiara Fasciani,^a M. Luisa Marin,^{a,c} Geniece L. Hallett- Tapley,^a and Juan C. Scaiano^{a*}

Solid niobium oxides and niobium phosphate were used as heterogeneous acid catalysts to promote the condensation between a switchable oxazine and a fluorescent coumarin in aprotic solvent. The niobium-based materials promote the generation of an active methylene from the

15 enamine-based portion of the oxazine, which is followed by nucleophilic attack on the aldehydic functionality of the coumarin reagent. Within the resulting system, the emission of the conjugated fluorophore can be observed at 670 nm and, thus, the processes occurring at the catalyst surface can be monitored in real time by Total Internal Fluorescence Microscopy (TIRFM).

20

A. Introduction

5 Halochromic compounds switch between differently colored states in response to a change in the pH of their surroundings. Often, halochromic behavior is accompanied by the possibility of tuning the structural and the electronic properties of molecules with light (photochromism) or heat (thermochromism).¹ Spiropyrans and oxazines, for instance, can undergo isomerization between two states with distinctive characteristics either by light or chemical stimulation.² The interplay between the means for interconversion and modulation of these systems offers the possibility for advanced applications.^{3,4,5,6}

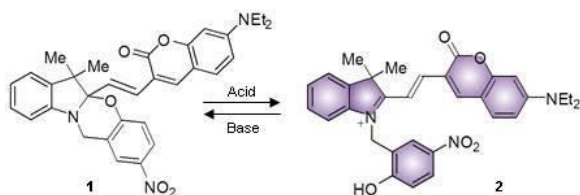
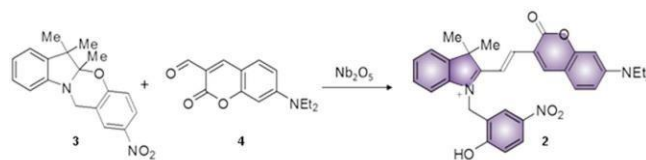


Figure 1. Halochromic interconversion between 1 and 2.

35 In a recent publication, we investigated the Brønsted acidic properties⁷ of several types of Nb₂O₅·*n*H₂O, including both commercially available and synthesized materials. Furthermore, we exploited these solids to activate the fluorescence of the halochromic assembly 1 (Figure 1).⁸ The chemical conjugation of a switchable oxazine and a fluorescent coumarin in compound 1 generates a 40 bimolecular system, in which the fluorescence of the latter at 670 nm can be turned on in association with the acid-induced ring opening

reaction of the halochromic unit (compound 2 in Figure 1).⁹ Single-molecule fluorescence techniques were successfully used to determine the rate of the protonation 1→2 and to obtain a detailed map of the Brønsted acid sites of the catalysts. The switchable assembly can be synthesized in a single step from precursors 3 and 4 (Figure 2). The conventional protocol consists of refluxing the reagents in a polar protic solvent, such as methanol or ethanol, upon the addition of several equivalents of an acid catalyst (trifluoroacetic acid, TFA) for over 24 hours; with this method, the product can be obtained in moderate yields (*ca.* 40% after purification by column chromatography).⁹



55 Figure 2. Proposed Nb₂O₅ catalyzed condensation between oxazine 3 and coumarin 4 to generate the fluorescent halochromic assembly 2.

We envisaged the possibility of using solid niobium oxides as potential heterogeneous acid catalysts with activity in polar aprotic solvents, such as acetonitrile (MeCN), to promote the C-C bond formation between 3 and 4 to directly generate the fluorescent conjugated assembly 2 (Figure 2). Specifically, we used two commercially available catalysts, hydrated Nb₂O₅·*n*H₂O (**T-I**) and niobium phosphate (**T-II**), and the mesoporous Nb₂O₅·*n*H₂O (**T-III**), which was prepared according to our recently published protocol.⁸ In addition to their known acidity properties, niobium oxides offer the added advantage of facile removal from the reaction mixture, as

compared to conventional homogeneous catalysts, as well potential reusability. Moreover, the use of aprotic solvents, such as MeCN, allows for the investigation of a potential solvent-like role of the niobium oxide acidic sites in reactions that traditionally require polar protic solvents. The condensation reaction can be carried out at moderate temperatures (45°C) for approximately 15 hours to obtain in a range of yields that strongly depend on the type of niobium oxide used in the preparation. The fluorescence of the generated assembly allows the catalyzed condensation between **3** and **4** to be monitored *in situ* and in real time with Total Internal Reflection Fluorescence Microscopy (TIRFM) on the catalyst surface.

B. Experimental

Materials

Compounds **1**, **3** and **4** were prepared according to literature procedures.^{9, 10} Commercial niobium oxides types I (**T-I**, hydrated Nb₂O₅·*n*H₂O) and II (**T-II**, niobium phosphate) were kindly provided by CBMM Brazil. Mesoporous Nb₂O₅·*n*H₂O type III (**T-III**) was prepared according to our recently published protocol (**T-IIIb** in Ref. 8). The acidity of the niobium oxide materials was estimated using conventional Hammett acidity indicator tests;¹¹ the procedure and the indicators have been described elsewhere.⁸ The p*K*_a ranges of the catalysts are reported in Table S1 of the Supporting Information.

Methods

MeCN was purified with a LC Technology Solutions Inc. SPBT-1 Bench Top Solvent Purification System. All chemicals were purchased from Sigma-Aldrich. All the reactions were monitored by thin-layer chromatography, using aluminum sheets coated with silica (60, F₂₅₄). NMR spectra were recorded at room temperature with a Bruker Avance 300. Mass spectra analysis was performed with a 6890N Network GC System equipped with a 5973 Mass Selective Detector from Agilent Technologies. High-resolution mass spectra were acquired with a HRes, EI, Concept S1, Magnetic Sector mass spectrometer and were conducted in the John L. Holmes Mass Spectrometry Facility at the Department of Chemistry, University of Ottawa. Absorbance spectra were recorded using a Cary 50 UV-visible spectrophotometer. HPLC analysis was performed with a Waters Integrity HPLC system coupled to a Waters 996 photodiode array detector. Reverse phase chromatography was achieved using a reverse phase Zorbax C18 column and an eluent mixture of MeOH and MeCN (4:6) with a flow rate of 0.25 mL/min in the presence of a standard (Coumarin 6, **C₆**). For HPLC analysis, 10 equivalents of Et₃N were added to each sample (the number of equivalents was calculated with respect to the theoretical yield of the product). Retention times: 11.8 min (**4**); 13.5 min (**3**); 17 min (**1**); 19.7 min (**C₆**), λ_{Obs} = 413 nm.

Single-Molecule Fluorescence Microscopy

The acid-catalyzed reaction measured at the single molecule level was performed in a reaction chamber with an area of 4.2 cm²/well (Thermo Scientific). **T-III** was dispersed in methanol and deposited on a clean coverslip (18 mm × 18 mm; Fisher

Scientific) through spin coating (1000 rpm, 40 s). The catalyst-loaded coverglass was then submerged in 1.0 mL of the reaction solvent, generated by mixing 255 μL of an 8.2 mM solution of **3** and 800 μL of a 2.6 mM solution of **4** in EtOH. Single molecule fluorescence imaging was carried out with a TIRF Olympus FV1000 (Olympus, Japan) microscope. A Chroma ZT640 dichroic mirror (Chroma Technology Corporation, Bellows Falls, USA) was used to reflect the 633 nm He-Ne (CW) excitation light into the 100x, 1.45 NA oil immersion Olympus Plan Apo objective (Olympus, Japan). The power density of the excitation laser at the sample was estimated to be 40W/cm². The Chroma ET600 excitation and Chroma ET655 emission filters (675/50 nm band-pass) allowed for optimum signal detection. The fluorescent signal was collected with the same objective and focused onto a Rolera EM-C² EM-CCD camera (Q-Imaging, Surrey, Canada) with 1004 x 1002 pixels of 8 x 8 μm size, operated at 50 ms per frame. The pixel size is 156 nm. Fluorescence spectra were recorded with a Fluorescent Lifetime Imaging System (PicoQuant, Berlin, Germany). The instrument is equipped with a frequency doubled, picosecond pulse diode laser (637 nm, 93 ps, 40 MHz, LDH-P-FA-640L; PicoQuant). The laser beam was collimated and focused through a fiber-coupling unit. A beam splitter (Z638rdc, Chroma) was used to separate excitation and emission light. The emission signal was collected by a Shemrock SR-163 spectrograph (Andor Technology, South Windsor, USA) using a 690/70 nm band-pass emission filter.

C Results and Discussion

For all reactions, equimolar amounts of **3** and **4** were dissolved in EtOH or MeCN. Upon the addition of the catalyst, the mixture was stirred vigorously for 15 h at 45°C, centrifuged and the supernatant was analyzed by HPLC upon addition of Et₃N. Due to its charged nature, the direct product of the condensation (**2**) possesses a high affinity for the HPLC stationary phase and cannot be eluted into the detection system under reverse phase conditions. Nonetheless, due to its intrinsic halochromic nature, the product **2** can be switched to its closed form (**1**) by the addition of base (see Figure 1), in which the absence of charged centers allows easy quantification of the yields by liquid chromatography. Results are reported in Table 1. Each **T-III** residue was stirred at room temperature in MeCN in the presence of Et₃N for 48h to encourage desorption of any reagents or products that might have been incorporated into the mesoporous structures. The mixture was again centrifuged (complete detachment was confirmed by lack of coloration of the catalysts), and the supernatant was dried, re-dissolved in a known volume of MeCN and analyzed by HPLC.

Table 1. % yields of the Nb₂O₅·*n*H₂O catalyzed condensation reaction between **3** and **4** to form **2**.^a

Catalyst	Amount of Catalyst	Solvent	Temperature (°C)	% of 1 ^a
----------	--------------------	---------	------------------	----------------------------

T-I	5 mg	MeCN	45	7.5
T-II	5 mg	MeCN	45	34
T-II	25 mg	MeCN	45	30
T-III	5 mg	EtOH	45	7
T-III	5 mg	MeCN	45	19
T-III	25 mg	MeCN	45	16
T-III	50 mg	MeCN	45	19
TFA	10 eq.	EtOH	80	38
TFA	10 eq.	MeCN	45	No product observed
No acid catalyst	-	EtOH or MeCN	45	No product observed

^aThe condensation product **2** was quantitatively converted into its neutral closed form **1** in order to perform HPLC analysis. For all reactions, peaks belonging to starting materials **3** and **4** are observed.

The condensation between **3** and **4** requires several steps, according to the mechanism described in Figure 3. The acid-induced cleavage of the C-O bond at the spirocenter in **3** generates the indolium cation **3a**, which forms the enamine **3b** upon elimination of a proton. Enamines can be considered as nitrogen analogues of enolates; their reactivity as nucleophiles is due to the dipolar character of one of the resonance structures (**3b'**), where the carbon in β position with respect to the nitrogen has a partial negative charge. The aldehyde appendage in **4** then reacts with the active methylene group of the heterocyclic cation of **3b'**, followed by proton transfer from the solvent and elimination of H₂O, with subsequent formation of the double bond between the two units. The proposed mechanism is in agreement with the conventional synthetic procedure, which consists in refluxing the reagents in MeOH or EtOH in the presence of trifluoroacetic acid (TFA).

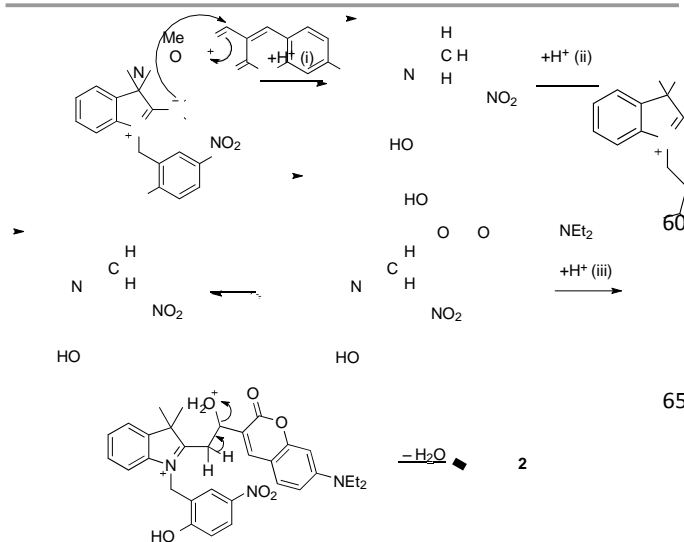


Figure 3. Proposed mechanism for the acid-induced condensation of **3** and **4** to yield **2**: acid-induced ring opening of **3** (i), removal of a proton (ii), nucleophilic attack of the aldehyde functionality in **4** from the active methylene in **3b'** and subsequent proton transfer from the solvent (iii), and elimination of H₂O.

The purpose of the acid within the homogeneous system is primarily to generate the active protonated ring-open structure **3a**, as well as protonating the reactive carbonyl in **4**, while the participation of protic solvents is required for the subsequent series of intermolecular proton transfers (ii and iii). High temperature favors the elimination of water.

Based on these considerations and the results reported in Table 1, we can provide insights into the mechanistic participation of different niobium oxides that were tested. Niobium phosphate (**T-II**) shows the highest activity, followed by the mesoporous type **T-III**. Both catalysts possess strong Brønsted-type acidity, thus are able to promote the first step of the reaction and open the spiro-center in **3** and, as previously observed,⁸ in **1**. According to Table S1, the acidity of these catalysts can be easily correlated to the efficacy of the overall reaction.

The use of a protic solvent in the conventional preparation allows for a continuous transfer of protons to/from the solvent itself and, therefore, plays an active role in the following steps of the reaction (Figure 3). No product is formed if MeCN is used in combination with a homogeneous acid catalyst (TFA). ¹H NMR spectra of **3** in CD₃CN and CD₃OD (Figure S1 and S2, Supporting Information) confirm that, upon the addition of TFA, the ring-opened species **3a** is generated in both solvents. Nonetheless, the chemical shift of the active methyl Me^a in **3a** (Figure 4) is located, as expected, significantly downfield in CD₃CN (2.84 ppm, Figure S1) with respect to CD₃OD (1.25 ppm, Figure S2). These results seem to indicate that the protons of Me^a remain significantly shielded when a protic solvent is used and that, in turn, hydrogen bonding is likely responsible for countering the electronic withdrawing effect of the indolium cation. Addition of CD₃OD to **3a** in CD₃CN promotes hydrogen bonding and, thus, the chemical shift of Me^a moves upfield and resembles its signal in pure CD₃OD (Figure S3, Supporting Information).

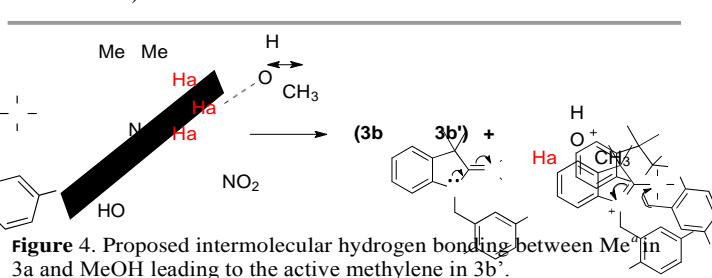


Figure 4. Proposed intermolecular hydrogen bonding between Me^a in **3a** and MeOH leading to the active methylene in **3b'**.

The formation of intermolecular hydrogen bonding with a protic solvent allows for the eventual continuous exchange of protons required to bring the overall reaction to completion. Yet, the presence of niobium oxides allows relatively good yields in MeCN. Thus, the efficiency of these catalysts, with respect to this particular reaction, must be related not only to their intrinsic Brønsted acidity, but also to their ability to participate in intermolecular hydrogen bonding and proton transfer, in a similar fashion as in Figure 4. This ability will, in turn, depend on hydration of the material,⁸ and/or on the accessibility of such proton-active sites. In the context of niobium oxides acidity, hydration would be considerably larger

in both **T-II** and **T-III** due to the enhanced acidity of these materials, as Brønsted acidity is known to be directly correlated to water content. These properties can directly translate into a higher probability of active proton transfer and, thus, higher reaction yields when the condensation reaction to form **2** is carried out in MeCN.

Although the activity of **T-II** and **T-III** are comparable by Hammett acidity testing, the yields obtained when using **T-III** as a catalyst are consistently lower than when **T-II** was employed. The decreased yield observed when using Nb₂O₅·nH₂O **T-III** is strongly dependent on the accessibility of the catalytic protonating sites. Given the mesoporous nature of catalyst **T-III**, it is likely that a considerable portion of the active proton sites is embedded within the cavities of the solid-state matrix, similar to the known properties of acidic faujasite Y zeolites.¹² In all cases, the susceptibility of any given substrate to do acid catalysis within the zeolite matrix is determined by the ability of the molecule to efficiently diffuse within the pores to the active site of the material. A similar situation can be envisioned within the mesoporous system of Nb₂O₅·nH₂O **T-III**. In such a case, it is plausible that several molecules of substrate **3** can diffuse within the pores and react with the active acid sites of the matrix. Indeed, one major disadvantage of employing porous heterogeneous catalysts involves the ability of substrate molecules to react with the acidic sites at the openings or entrance points to the matrix pores. As a result, the three-dimensional pores may become blocked rendering the remaining catalytic acid sites embedded within the mesoporous structure inaccessible for catalytic conversion and translate into lower yields of product, as was observed for mesoporous catalyst **T-III** presented in Table 1. In alternative, the lower yields observed for **T-III** may also be due to the spatial constraints within the mesoporous system and the inability of the material to accommodate the speculated large transition state of the oxazine/coumarin adduct. In other words, beyond the acidity of a given site, the traffic that enables molecules to reach the site and ultimately depart from it are key parameters in the case of mesoporous catalysts.

Interestingly, in the presence of the niobium oxide, the reaction in MeCN is much more efficient than in EtOH. This is possibly due to a partial solvation effect from the EtOH of the active sites of the catalyst; indeed, if EtOH molecules are arranged through intermolecular hydrogen bonding interactions with the proton-like moieties on the surface of the niobium oxide, the activity of the solids may be dramatically reduced.

Catalysis at the Single Molecule Level

The dynamics of the acid-catalyzed condensation between **3** and **4** was monitored *in situ* using TIRF microscopy. Previously we observed that, upon protonation, **1** yields a sufficiently fluorescent product (**2**) that can be easily detected at the single molecule level over the Nb₂O₅·nH₂O catalyst.⁸ With an excitation wavelength of 633 nm and emission band pass filter of 675/50 nm, only the product of the condensation can be selectively excited and observed. (Full spectroscopic

characterization of **1** and **2** and the starting materials **3** and **4** can be found in the Supporting Information, Figure S4 and S5). The accumulated fluorescence intensity image of a movie recorded for 25 s shows spatially scattered distribution for the catalytic formation of **2** (Figure 5).

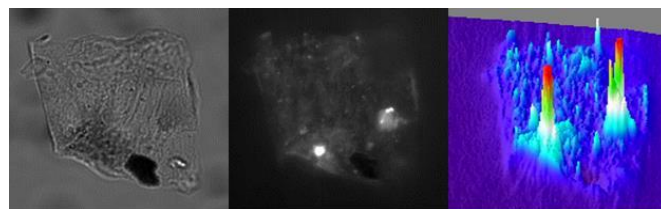


Figure 5. Transmission (left), TIRF (center) and 3D (right) images of a T-III particle immobilized on a cover glass and immersed in a 2 mM solution of **3** and **4** with 633 nm laser excitation (see Supplementary Video S1) and a 675/50 nm band pass emission filter. The fluorescence image and the 3D representation correspond to the accumulated spot intensity reconstructed from a movie of 500 frames in length (50 ms per frame).

Typical time-dependent fluorescent intensity traces of **2** (Figure 6) proves that the individual product molecules can be easily distinguished from background signals caused by scattering or fluorescence of the catalyst surface and from the high concentrated reactant solution, respectively. Characterization of the bright spots was performed by measuring their emission spectra *in situ* (Figure 6), which is ascribed to product **2**.

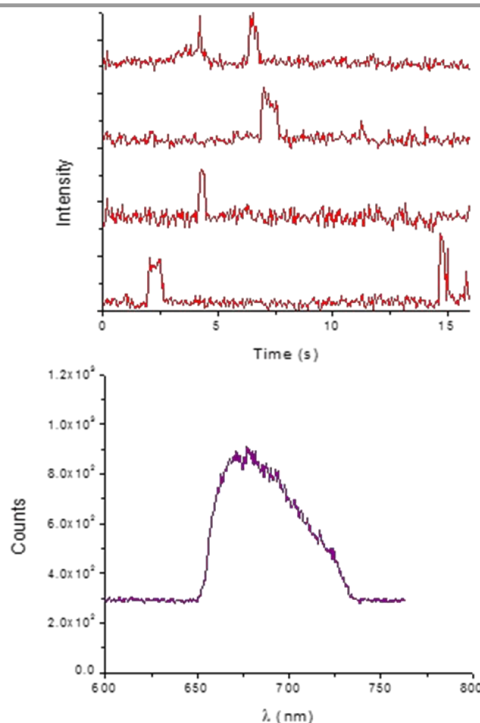


Figure 6. On top: Typical fluorescence intensity trajectories observed for the "turn ON" of molecules of **2** over a T-III particle. On the bottom: Spectral information of the detected bright spots during "turn ON" events measured by passing the epi fluorescent signal through a spectrograph ($\lambda_{\text{ex}} = 637 \text{ nm}$) and using a 690/70 nm band pass emission filter installed into the Fluorescent Lifetime Imaging System.

Through the analysis of the number of single “turn ON” events of fluorescent molecules over the catalyst (for a total of six different **T-III** particles), the typical observation rate was found to be 8 molecules per $100 \mu\text{m}^2$ over a period of 25 s, corresponding to $5 \times 10^{-15} \text{ mol m}^{-2} \text{ s}^{-1}$ for the reaction between equimolar amounts of **3** and **4**. This rate is representative of the overall mechanism described in Figure 3, which includes the initial adsorption and protonation of **3** and the subsequent condensation between the ring-open active **3c** with **4** to yield **2**. 3D surface maps of the TIRFM sequence (Figure 7) depict the catalytic “hot spots” of **T-III**, characterized by the highest acidity and, considering the mesoporous nature of the catalyst, easiest accessibility.

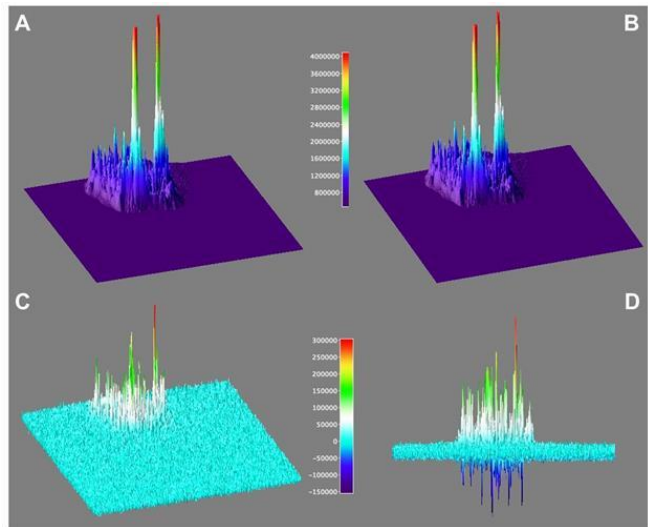


Figure 7. Catalytic activity of a **T-III** particle for the overall condensation of **3** and **4** to generate **2** (see Figure 2) by detection of the fluorescence of **2** by TIRFM. Surface maps A and B show the accumulated signal for 12.5 seconds and the subsequent 12.5 seconds, while C and D show the rescaled difference of A minus B (see color coded legend) from different perspectives.

20 Reusability Experiments

Heterogeneous catalysts have the advantage of allowing their easy and inexpensive removal from reaction mixtures by filtration or centrifugation. Due to these reasons, a catalyst can often be recovered and used for multiple reaction cycles, provided that its efficiency has not been compromised by previous uses. Thus, the reusability of **T-II** was tested for the condensation between **3** and **4**. Indeed, **T-II** resulted to be the most efficient catalyst for the generation of **2**, and the lack of surface adsorption of the latter on the heterogeneous surface allowed simpler and faster separation than the mesoporous **T-III**. In all instances, after centrifugation, separation and analysis of the supernatant phase, **T-II** was washed three times with MeCN, centrifuged, dried overnight in a fume hood and used “as is”. The recyclability results are depicted in Figure 8.

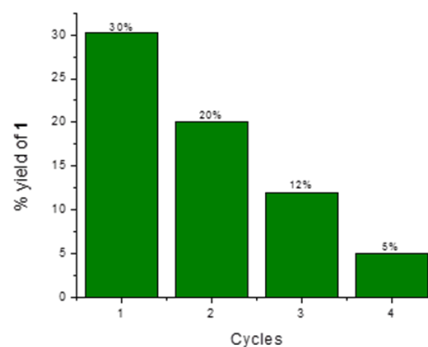


Figure 8. Recyclability of **T-II** for the acid-catalyzed condensation of between **3** and **4**.

Conclusions

We have successfully demonstrated that solid niobium phosphate and mesoporous $\text{Nb}_2\text{O}_5 \cdot n\text{H}_2\text{O}$ (**T-II** and **T-III**, respectively) have the ability of promoting complex reactions such as the condensation between enamine-like moieties and aldehydes. In particular, the role of the niobium oxide catalysts in several reaction steps was investigated. Based on our results, we conclude that, in addition to the known and previously reported Brønsted acidity (required in the first step of the reaction), niobium oxides can adopt solvent-like behavior, specifically in the formation of hydrogen bonding interactions and the participation in intermolecular proton transfers. Selecting reagents which, once assembled, can generate a species with suitable emission wavelength and quantum yield, the reaction can be monitored with single molecule techniques. Using TIRFM and monitoring bursting fluorescent events on the surface of the catalyst, the rate constant for the reaction between **3** and **4** to yield **2** was found to be $5 \times 10^{-15} \text{ mol m}^{-2} \text{ s}^{-1}$. In addition, 3D surface mapping techniques were used to illustrate catalytic hot spots of the niobium oxide **T-III**, and their evolution over time.

Acknowledgements

The authors wish to thank the Natural Sciences and Engineering Research Council (NSERC) and the Canada Research Chairs program. The University of Ottawa International Office provided grants to study niobium. Thanks are due to the Government of Canada and NSERC for a Banting Postdoctoral Fellowship to S. Impellizzeri and a Vanier Scholarship to C. Fasciani. S. Simoncelli acknowledges a DFAIT fellowship from ELAP (Emerging Leaders in the Americas Program) to support her visit to Canada. M. L. Marin thanks the financial support of the Generalitat Valenciana (BEST/2012/233) and the

Distinguished Visiting Professor program of the University of Ottawa.

Notes and references

- ^a Department of Chemistry, Centre for Catalysis Research and Innovation, University of Ottawa, 10 Marie Curie, Ottawa, Ontario K1N 6N5, Canada. Email: Scaiano@photo.chem.uottawa.ca
- ^b INQUIMAE and Departamento de Química Inorgánica, Analítica, y Química Física, Facultad de Ciencias Exactas y Naturales, Universidad de Buenos Aires, 1428 Buenos Aires, Argentina
- ^c Instituto Universitario Mixto de Tecnología Química (UPV-CSIC), Universitat Politècnica de València. Avenida de los Naranjos s/n, 46025 Valencia, Spain
- †Electronic Supplementary Information (ESI) available: Hammett acidity (H_0) for the niobium catalysts employed for the condensation of **3** and **4**; ¹H NMR of **3** in CD₃CN before and after the addition of TFA; ¹H NMR of **3** in CD₃OD before and after the addition of TFA; ¹H NMR (detail) of **3a** in CD₃CN after the addition of CD₃OD; Normalized absorption spectra of compounds **1-4**; Emission spectra of compounds **1-4**.
1. B. L. Feringa, *Molecular Switches*, Wiley-VCH, Weinheim, 2001.
 2. J. C. Crano and R. J. Guglielmetti, *Organic Photochromic and Thermochromic Compounds*, Plenum Press, New York, 1999.
 3. A. S. Dvornikov, J. Malkin and P. M. Rentzepis, *The Journal of Physical Chemistry*, 1994, **98**, 6746-6752; A. S. Dvornikov, E. P. Walker and P. M. Rentzepis, *The Journal of Physical Chemistry A*, 2009, **113**, 13633-13644; M. Irie, *Chemical Reviews*, 2000, **100**, 1683-1890; D. A. Parthenopoulos and P. M. Rentzepis, *Science*, 1989, **245**, 843-845.
 4. V. Balzani, A. Credi and M. Venturi, *Molecular Devices and Machines: Concepts and Perspectives for the Nanoworld*, Wiley-VCH, Weinheim, 2008; A. P. de Silva, N. D. McClenaghan and C. P. McCoy, in *Electron Transfer in Chemistry*, ed. V. Balzani, Wiley-VCH, Weinheim, 2001, pp. 156-185; F. M. Raymo, *Advanced Materials*, 2002, **14**, 401-414; F. M. Raymo, R. J. Alvarado, S. Giordani and M. A. Cejas, *Journal of the American Chemical Society*, 2003, **125**, 2361-2364; F. M. Raymo and S. Giordani, *Organic Letters*, 2001, **3**, 3475-3478; F. M. Raymo, S. Giordani, A. J. P. White and D. J. Williams, *The Journal of Organic Chemistry*, 2003, **68**, 4158-4169; S. Silvi, E. C. Constable, C. E. Housecroft, J. E. Beves, E. L. Dunphy, M. Tomasulo, F. M. Raymo and A. Credi, *Chemistry – A European Journal*, 2009, **15**, 178-185.
 5. J. Cusido, S. Impellizzeri and F. M. Raymo, *Nanoscale*, 2011, **3**, 59-70; S. W. Hell, *Nat Meth*, 2009, **6**, 24-32; F. M. Raymo, *The Journal of Physical Chemistry Letters*, 2012, **3**, 2379-2385; M. Sauer, *Proceedings of the National Academy of Sciences of the United States of America*, 2005, **102**, 9433-9434.
 6. E. Deniz, M. Tomasulo, J. Cusido, I. Yildiz, M. Petriella, M. L. Bossi, S. Sortino and F. M. Raymo, *The Journal of Physical Chemistry C*, 2012, **116**, 6058-6068; D. Hu, Z. Tian, W. Wu, W. Wan and A. D. Q. Li, *Journal of the American Chemical Society*, 2008, **130**, 15279-15281; M. Petriella, E. Deniz, S. Swaminathan, M. J. Roberti, F. M. Raymo and M. L. Bossi, *Photochemistry and Photobiology*, 2013, **89**, 1391-1398; B. Seefeldt, R. Kasper, M. Beining, J. Mattay, J. Arden-Jacob, N. Kemnitz, K. H. Drexhage, M. Heilemann and M. Sauer, *Photochemical & Photobiological Sciences*, 2010, **9**, 213-220.
 7. I. Nowak and M. Ziolk, *Chem. Rev.*, 1999, **99**, 3603-3624; S. Okazaki and A. Kurosaki, *Catal. Today*, 1990, **8**, 113-122; S. Okazaki and N. Wada, *Catal. Today*, 1993, **16**, 349-359; T. Ushikubo, I. Iizuka, H. Hattori and K. Tanabe, *Catal. Today*, 1993, **16**, 291-295.
 8. M. L. Marin, G. Hallett-Tapley, S. Impellizzeri, C. Fasciani, S. Simoncelli, J. C. Netto-Ferreira and T. Scaiano, *Catalysis Science & Technology*, 2014.
 9. E. Deniz, S. Sortino and F. M. Raymo, *The Journal of Physical Chemistry Letters*, 2010, **1**, 3506-3509.
 10. M. Tomasulo, S. Sortino, A. J. P. White and F. M. Raymo, *The Journal of Organic Chemistry*, 2005, **70**, 8180-8189; J.-S. Wu, W.-M. Liu, X.-Q. Zhuang, F. Wang, P.-F. Wang, S.-L. Tao, X.-H. Zhang, S.-K. Wu and S.-T. Lee, *Organic Letters*, 2006, **9**, 33-36.
 11. I. Matsuzaki, M. Nitta and K. Tanabe, *J. Res. Inst. Catalysis, Hokkaido Univ.*, 1969, **17**, 46-53; M. Yurdakoc, M. Akcay, Y. Tonbul and K. Yurdakoc, *Turk. J. Chem.*, 1999, **23**, 319-327.
 12. A. Corma and A. Martinez, *Adv. Materials*, 1995, **7**, 137-144; S. Corrent, P. Hahn, G. Pohlers, T. J. Connolly, J. C. Scaiano, V. Fornés and H. García, *J. Phys. Chem. B*, 1998, **102**, 5852-5858; J. C. Scaiano and H. García, *Acc. Chem. Res.*, 1999, **32**, 783-793.